Internal Dynamics and Energy Transfer in Dansylated POPAM Dendrimers and Their Eosin Complexes

Jukka Aumanen,*,† Tero Kesti,‡,# Villy Sundström,‡ Gilberto Teobaldi,⊥,¶ Francesco Zerbetto,⊥ Nicole Werner,§ Gabriele Richardt,§ Jeroen van Heyst,§,& Fritz Vögtle,§ and Jouko Korppi-Tommola†

Department of Chemistry, Nanoscience Center, University of Jyväskylä, P.O. Box 35, 40014 Finland, Department of Chemical Physics, Chemical Center, Lund University, Box 124, SE-22100 Lund, Sweden, Kekulé-Institut für Organische Chemie und Biochemie der Rheinischen, Friedrich-Wilhelms-Universität Bonn, Gerhard-Domagk Strasse 1, 53121 Bonn, Germany, and Department of Chemistry "G. Ciamician", University of Bologna, V.F. Selmi 2, 40126 Bologna, Italy

Received: March 31, 2009; Revised Manuscript Received: November 26, 2009

Internal dynamics of dansylated poly(propyleneamine) dendrimers (POPAM, G1−G4) in solution and excitation energy transfer from dansyls to eosin in POPAM−eosin complexes have been studied by time-resolved fluorescence spectroscopy and molecular dynamics (MD) simulations. Combining the results from fluorescence anisotropy and the MD simulation studies suggests three time domains for the internal dynamics of the G3 and G4 generations, about 60 ps for motions of the outer-sphere dansyls, 500−1000 ps for restricted motions of back-folded dansyls, and 1500−2600 ps for the overall rotation. For the smaller generations, the contribution from the restricted motions was not entirely evident. Eosin binding hinders fast rotation of the dansyl fragments in the largest G4 dendrimer, but the motion of back-folded dansyls is more hindered in the pure dendrimer. Both fluorescence anisotropy and MD results for the G4 dendrimer support the "soft" dendrimer picture with almost free mobility and substantial back-folding of the dansyls of the dendrimers in solution. Analysis of time-dependent spectral shifts of fluorescence reveals 20−30 ps excited-state solvation relaxation around a single dansyl of a dendrimer. Dendrimer-independent excitation energy transfer from 4 to 8 ps from dansyls to eosins in POPAM−eosin complexes G2−G4 was observed.

Introduction

Multibranched highly symmetric dendritic molecules have attracted increasing scientific attention in recent years. Not only the structural beauty of the molecules but also the range of possible applications has been a motivation for chemists to synthesize and investigate structural and dynamic properties of dendrimers.[1−3] A rapidly expanding field of research is the use of dendrimers for drug delivery as they can be tailored to bind the desired drug molecule and for targeted delivery.[4−7]

Dendrimers can be used for light harvesting by introducing light absorbers into the periphery of the dendrimer. Several dendrimers having ligands absorbing in the range from UV to the visible spectral region have been synthetized. Dansylated poly(propyleneamine) dendrimers (POPAM) are efficient UV light harvesters.[8] Dansyl substitution is widely used, for example, in biological labeling due to the ability of dansyl chloride to react with free amino groups in proteins to form highly fluorescent species. Dansyl-labeled compounds have a very large Stokes shift, and their fluorescence properties (emission wavelength and quantum yield) are sensitive to the environment.[9,10] Absorption properties of dansylated POPAMs calculated per chromophore are surprisingly similar, an indication of relatively weak interaction between the chromophores, even in the largest generation studied.[8]

Several fundamental properties of dendrimers have been studied, including structural,[11−14] luminescent,[15−22] and dynamic properties,[23−33] self-assembly,[2,34] and light harvesting.[27,35,36] A number of structural studies of dendrimers have been presented based on the results from small-angle X-ray (SAXS) and neutron scattering (SANS) data and theoretical predictions.[11−14,37,38] Two structural concepts have been established, the "soft" or dense core dendrimer and the stiff or dense shell dendrimer. In the former group, dendritic end groups may back-fold, and the highest monomer density is accumulated in the center.[11,12,14] In stiff dendrimers, only small-amplitude motion of the peripheral groups is possible, and the center monomer density is low as compared to the peripheral density.[13] Monte Carlo (MC) and molecular dynamics (MD) simulations[39,40] suggest that high atom density in a soft dendrimer may also accumulate in the outer shell at high pH, while at low pH, a globular, back-folded structure prevails. Assuming that a small guest molecule (a drug) could be complexed with the dendrimer at low pH, one then could imagine the guest to be released via the structural rearrangement process when the pH of the system is increased.

One of the most important experimental techniques to study monomer distributions in dendrimers is the small-angle neutron scattering (SANS) method. Scattering from the peripheral groups may be greatly enhanced by deuteration of these groups in

* To whom correspondence should be addressed. E-mail: jukka.aumanen@jyu.fi.
† University of Jyväskylä.
‡ Lund University.
⊥ University of Bologna.
§ Friedrich-Wilhelms-Universität Bonn.
# Current address: Measurement and Sensor Laboratory, University of Oulu, Technology Park 127, FIN-87400 Kajaani, Finland.
¶ Current address: Surface Science Research Centre, Department of Chemistry, University of Liverpool, L69 3BX Liverpool, U.K.
& Current address: Materials Science Department - Polymer Chemistry, Swiss Federal Institute of Technology (ETH)—Zürich, Wolfgang Pauli Strasse 10, HCI H 528, CH-8093 Zürich, Switzerland.

10.1021/jp902906q
Published on Web 01/08/2010

conjunction with the solvent contrast variation and monomer distribution obtained.[11] Yet, contradicting interpretations from such experiments in polar solutions have been reported for soft dendrimers.[12,41] In the study of a poly(amidoamine) (PAPAM) G7 dendrimer,[41] the larger radius of gyration (39 Å) obtained for the partially deuterated dendrimer as compared to the corresponding radius of the nondeuterated dendrimer (34 Å) was considered as evidence for accumulation of the terminal groups in the periphery. Soon afterward, it was theoretically shown that the radius of gyration of a dendrimer when calculated only from the terminal units is larger than the radius calculated for the three-dimensional simulated structure of the dendrimer.[42] This result means that the radius of gyration may not be used as a conclusive measure for spatial distribution of the terminal groups. In their SANS study of fully deuterated urea-functionalized poly(propyleneamine) (POPAM) G4, Rosenfeldt et al.[12] convincingly showed that the distribution of terminal groups had a maximum of around 2 nm, a result strongly suggesting that most of the end groups fold back, and the dense core picture is supported. It is noted that in the two SANS studies, solvents used were of different character, methanol[41] versus dimethylacetamide,[12] the former being more acidic than the latter. According to the results from the MC and MD simulations discussed above, dense shell structure could be slightly favored in methanol, while in amide solution, the structure would tend toward the dense core configuration. It is noted then that the experimental results still do not give unambiguous answers with regard to the distributions of the end groups in a dendrimer. In their review article, Ballauff and Likos[37] summarize that the dense core picture prevails for the majority of cases for soft dendrimers.

Small-angle neutron diffraction measurements give information on statistical ensemble averages of distributions of terminal groups of dendrimers, but the method is not able to give information on dynamics, overall rotation, or internal dynamics of dendrimers. On the theory side, MC and MD simulations may be used to characterize dynamic properties of dendrimes.[40,42−44] From such simulations, information on self-diffusion of dendrimers, on rotational motions of the dendrimer as a whole, on shape and size fluctuations, and on motions of individual monomers (terminal groups) may be obtained.[44] Two important results by analyzing the autocorrelation functions (ACF) of the bond vectors have been demonstrated: (1) at a given segment, the bond orientations slow down with dendrimer size, and (2) in a given dendrimer, orientations become faster as one moves away from the core. Distributions of relaxation times of the outer-shell bonds indicate at least two time domains, "short" (a few picoseconds) and "long" (on the order of 100 ps or longer). The long component has been assigned to the overall rotation of the dendrimer, while the short component has been assigned to bond reorientation.[45] Also, intermediate time regimes were resolved. Similar dual time behavior has been reported in a simulation of neutral dendrimers; the fast component was assigned to internal relaxation and the slow component to overall rotation of the dendrimer.[44]

There are a few experimental methods to obtain dynamic information on internal and overall motions of dendrimers, ^{13}C NMR relaxation measurements,[46] quasielastic neutron scattering,[47] and polarized luminescence methods.[20] In the pioneering work of Meltzer et al.[46] based on simulation of T_1 and NOE data of a PAPAM dendrimer, the dual behavior of relaxations of the intradendritic motions, slow interior and fast terminal relaxation, is shown. In particular, the intradendritic motions slowed down with the increasing size of the dendrimer.

For dendrimers containing emitting terminal groups, real time dynamics may be obtained by using polarized luminescence measurements. Upon excitation with a polarized ultrafast laser pulse, one creates a population of excited dendrimers having the transition moment of one of the terminal groups parallel to the excitation polarization. Recording the emission decay in the parallel and perpendicular directions with respect to the excitation polarization, the time dependence of the fluorescence anisotropy that contains contributions from the motions of terminal groups, internal motions, the overall rotation of the dendrimer, and excitation energy-transfer rates between the terminal groups may be evaluated. Time domains of these relaxation processes depend of the structure and generation of the dendrimer and the interaction strength between the terminal chromophores. In stiff dendrimers with chromophores in the periphery with strong or medium interaction, one expects an increase in intrachromophore excitation energy-transfer (EET) rates as the size of the dendrimer grows. In soft dendrimers, intradendritic motions play an important role, and the created anisotropy may decay due to internal motions, energy transfer between the groups, and overall rotation. In dendritic host−guest complexes, two EET channels may be operational simultaneously, that is, chromophore−chromophore EET and chromophore−guest EET. If a single guest molecule would reside in the core of a stiff dendrimer, then generation-dependent EET from excited chromophores to the guest would be observed. However, in soft dendrimers like POPAMs, where several guests may be present,[48] the situation becomes more complicated. If the guests were bound in the close proximity of the donors and the overlap of the donor emission and acceptor absorption were large, one then would see generation-independent EET.

Extensive work is available on ultrafast energy-transfer dynamics of phenylacetylene dendrimers.[23,24,26,27] UV excitation of the peripheral chromophores of these dendrimers resulted in excitation energy transfer toward the covalently bound trap, the central aromatic ring, on a subpicosecond time scale.[23,24] Subpicosecond EET rates from the coumarin periphery to a tetraphenylporphyrin acceptor has been reported in a first-generation dendrimer with EET efficiency exceeding 95%.[30] In carbonyl-terminated phenylacetylene dendrimers, the initial excitation has been observed to be delocalized in dendrons of the large dendrimers and such delocalization could either enhance or slow down EET. Intersite transfer times from 5 to 17 ps were reported for these dendrimers.[27] In multichromophore donor−acceptor dendrimers, directional EET and electron transfer (ET) have been observed.[29,31] For peryleneimide-substituted polyphenylene dendrimers, in addition to intradendrimer energy hopping, a photoinduced intramolecular and solvent-dependent electron-transfer process (short-lived ion pair state in polar solution and long-lived state in less polar solution) in the amine core was identified.[29] A special group of dendrimers is the one with porphyrin appended dendrimers.[49,50] As porphyrins are fairly large substituents (with possible $\pi-\pi$ interaction), spatial crowding in the higher generations becomes an issue. The chromophores of these dendrimers have been assumed to be randomly distributed on a spherical surface, and according to model simulations, rapid excitation transfer takes place between porphyrins situated on the surface, whereas slower EET involves porphyrins in dendrons outside of this surface.[32] Exciton−exciton annihilation studies of Zn-porphyrin dendrimers with 4−64 Zn-porphyrin chromophores suggest fast, 10 ps, next neighbor annihilation, while a slower component resolved was attributed to a sequential annihilation process with 100 ps EET hopping time.[31] Even for the largest dendrimer containing

CHART 1: Structural Formulas of the Reference Compound *N*-Propyldansylamine, the Guest Molecule Eosin Dye, and the Dansylated POPAM Dendrimers[a]

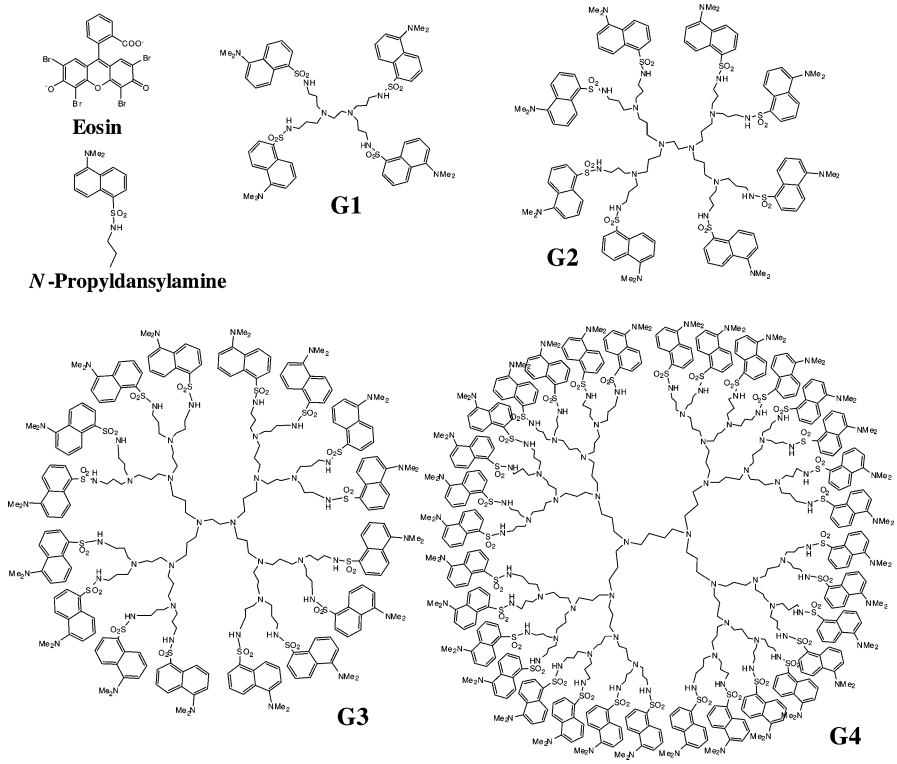

[a] G*n* ($n = 1-4$) refers to generation of the dendrimer.

64 Zn-porphyrins, it was concluded that efficient energy transfer occurs only between the chromophores of one dendron.

In order to use dendrimers as artificial light harvesting antennas or as a part of a functional device, directional excitation energy transfer from peripheral donors to an acceptor in a desired location of the dendrimer is needed. The acceptor could in principle be a covalently bound dendritic ligand,[23,36,51] a centrally located energy "sink" (lanthanoid or organic "seed" molecule)[19,28,30] or a weakly bound guest, either in a dendritic "pocket" or in the antenna periphery.[16,48,52,53] In the present paper, we use the characteristic property of POPAM dendrimers to host dyes via van der Waals and/or hydrogen-bonding interactions. Previously, it has been demonstrated that dansylated POPAMs can host xanthene dyes, such as eosin, which serve as efficient acceptors due to good overlap of the dansyl emission and eosin absorption spectra.[48] The exact binding sites of the eosins in the dendrimer backbone are not known, and molecular dynamics simulations were carried out to shed light on these sites and their dynamics. In addition intrachromophore distance distributions, radii of gyration, dynamics analysis of the motions of the individual dansyls, and overall rotation of the pure and complexed dendrimers were considered as important information for interpretation of the experimental anisotropy data.

In our previous paper,[54] we used transient absorption spectroscopy to study energy-transfer kinetics from the dansyls to eosin in POPAM−eosin complexes. Energy transfer was characterized by three time constants, 150 fs, 1 ps, and 5−7 ps, and was almost independent of dendrimer generation, indicative of close proximity of eosins to dansyl chromophores. In the transient absorption measurements, no stimulated emission signal from the dansyls could be seen, and the response to dansyl excitation could only be seen in eosin−POPAM complexes in the eosin bleach region. To obtain real time information on dansylated POPAM dendrimer dynamics in a polar solvent, chloroform, time-resolved fluorescence anisotropy measurements were carried out. An estimate for reorientation motions of the terminal dansyls was obtained by measuring the anisotropy decay of a reference compound *N*-propyldansylamine in the same solvent. It was hoped that fluorescence anisotropy results would bring new insights to internal dansyl dynamics and overall rotation of the dendrimers as well as dansyl to eosin excitation energy transfer in the complexes.

Experimental Section

Synthesis and characterization of dansylated POPAM dendrimers[8,55] and the *N*-propyldansylamine[56] reference compound used in this study have been described elsewhere. The 2D structural formulas of all studied compounds are presented in Chart 1. All dendrimer samples were dissolved in chloroform, and eosin was dissolved in ethanol. Dendrimer−eosin complexes were prepared by adding a droplet of highly concentrated eosin ethanol solution into a dendrimer solution and mixing vigorously. Using a small volume of ethanol solution prevented formation of two separate solvent phases. Absorbance in the center of both dansyl and eosin absorption bands was adjusted to be 0.6 in a 1 mm path length cell. This means a stoichiometric ratio of 1 eosin per 15 dansyls (absorption coefficients given by Balzani et al. were used for this estimation).[48]

For time-resolved fluorescence measurements, 400 nm excitation pulses were produced by frequency doubling the output of a Ti:Sapphire oscillator (Spectra-Physics Tsunami). The ratio of dansyl to eosin absorption was estimated to be about 10:1 at the excitation wavelength. A pulse picker was used to decrease the pulse repetition rate from 82 down to 4 MHz. Polarization of the excitation beam was adjusted with a Berek polarization compensator. Time-resolved fluorescence spectra were recorded with a streak camera (Hamamatsu C 4742-95). A spectral

window of 100 nm and three different time windows (50 ps, 200 ps, and 2 ns) were used to collect the data for each sample. In all cases, fluorescence polarized both parallel and perpendicular to the excitation light was recorded. Excitation fluences used in this study were much below the levels needed to photochemically decompose chloroform. Time correlated single photon counting (TCSPC) measurements were made by using a 385 nm diode laser as the excitation source, a multichannel plate detector and a commercial single photon counting data acquisition system (PicoQuant HydraHarp 400). Time resolution of the instrument was about 130 ps.

Molecular dynamics (MD) simulations were carried out via a modified Beeman algorithm as implemented in the TINKER program as previously used to study eosin (E) encapsulation and dynamics in dansylated POPAM dendrimers.[57] The adopted force field was MM3. MD trajectories were generated by sampling in a canonical ensemble (NVT) at $T = 298$ K. In all of the simulations, the integration time step was 1 fs, and no geometrical constraint was enforced with respect to the hydrogen atoms. The side of the (cubic) simulation cells was 61.416 Å. Four eosin (E) guests where simulated together with the fourth-generation dansylated POPAM dendrimer (G4). Both G4 and 4E@G4 were modeled in $CHCl_3$ under an infinite dilution approximation which yielded simulation cells of 8642 and 8640 atoms, respectively. Before data sampling, the solvent box (first) and the global systems (then) were equilibrated by means of a simulated annealing procedure (2000 and 298 K).

From the extended simulation of the MD trajectory, the dansyl rotational autocorrelation function (D_{RACF}) was calculated as

$$D_{RACF}(t) = \langle \phi_i(t)\phi_i(t_0)\rangle \quad (1)$$

where Φ_i define the N−S−C_{sp2}−C_{sp2} torsional angle of the i^{th} dansyl fragment. Conversely, the global dendrimer rotational autocorrelation function (D_{G4}) was calculated as

$$D_{G4}(t) = \langle \boldsymbol{\omega}_i(t)\cdot\boldsymbol{\omega}_i(t_0)\rangle \quad (2)$$

where $\boldsymbol{\omega}_i$ defines to the set of the (3) orientation cosines that the i^{th} atom forms with the (3) axes of the reference system (centered on the instantaneous dendrimer center of mass)

$$\boldsymbol{\omega}_i(t) = [\cos \omega_i^x(t), \cos \omega_i^y(t), \cos \omega_i^z(t)] \quad (3)$$

Both D_{RACF} and D_{G4} were calculated using blocks of 9000 points separated by 0.05 ps (450 ps) which were eventually averaged over 8000 (t_0) origins shifted by 0.25 ps.

Results

A. Dansylated POPAM Dendrimers. Dansylated POPAM dendrimers and the reference compound have the emission maximum at around 500 nm (Figure 1). Eight kinetic traces from different spectral regions of each streak image were analyzed. To increase signal-to-noise ratio, data from a 13 nm wide spectral strip were averaged into a single kinetic trace. Magic angle fluorescence was constructed from parallel and perpendicular traces by using a well-known equation

$$I_{mag}(t) = \frac{I_{||}(t) + 2I_{\perp}(t)}{3} \quad (4)$$

Dansyl fluorescence decays of the reference compound and the four POPAMs at three different wavelengths are shown in Figure 2. In contrast to the reference compound, all POPAMs show a fast wavelength-dependent decay component with reduction in amplitude when going from the blue side of the fluorescence spectrum to the red side. The rest of the decay

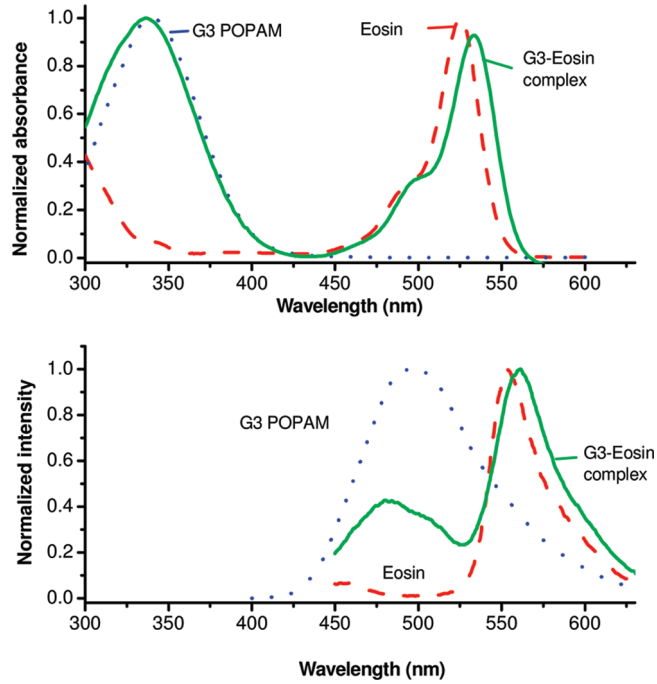

Figure 1. Normalized steady-state absorption (upper) and fluorescence (lower) spectra of the dansylated G3 POPAM dendrimer (blue, dot), eosin (red, dash), and the corresponding eosin complex (green, solid). The spectra of other generations are very similar to ones shown in the figure.

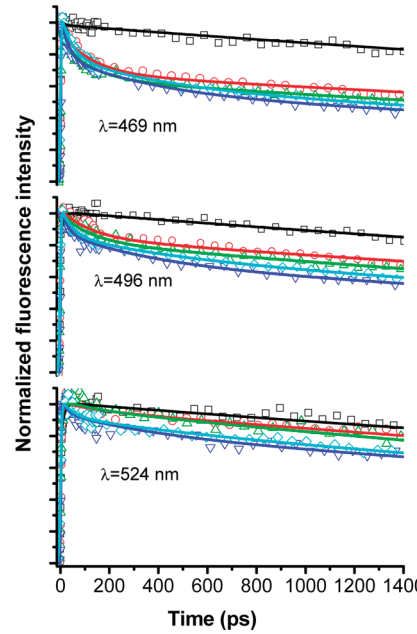

Figure 2. Magic angle dansyl fluorescence decay traces of the dansylated POPAM dendrimers in the blue, center, and red regions of the emission spectrum, G1 (red O), G2 (green Δ), G3 (blue ▽), and G4 (cyan ◇), and the reference compound *N*-propyldansylamine (black □).

profiles are independent of wavelength and fall in the nanosecond time domain.[58] The amplitude of the fast decay component slightly increases toward higher dendrimer generations. Figure 3 shows early parts of the G1 POPAM fluorescence rise and decay kinetics at three wavelengths. The decay on the blue side of the fluorescence spectrum appears as a rise when one moves to the red side, while in the center, the early part of the signal is more or less flat. The signal clearly turns from a decay to a rise in G1 and G2 POPAMs and the reference compound, while

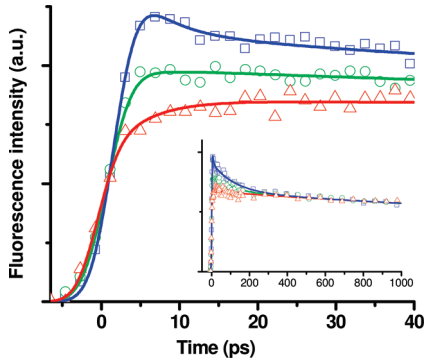

Figure 3. Early parts of the magic angle fluorescence kinetics of the G1 POPAM dendrimer at three different wavelengths, 469 (blue), 496 (green), and 524 nm (red).

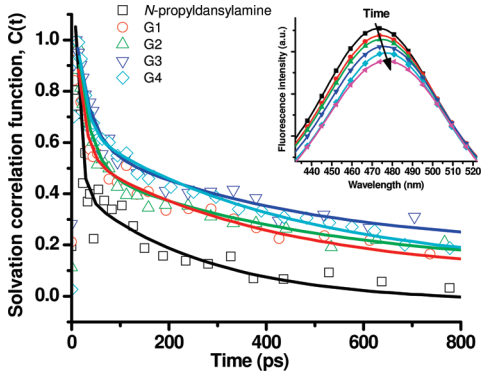

Figure 4. The solvation correlation functions, $C(t)$, for the dansylated POPAM dendrimers in chloroform at RT, G1 (red O), G2 (green Δ), G3 (blue ▽), and G4 (cyan ◇), and the reference compound (black □). The inset shows the time evolution of the G1 fluorescence spectrum. The shape of the spectrum did not change with time.

in larger POPAMs, only the amplitude of the fast decay component diminishes toward the red end of the spectrum.

Wavelength dependencies of the early fluorescence decay and rise signals are typical of excited-state solvent relaxation. The observed kinetic changes were analyzed by using a solvation correlation function $C(t)$,[59] defined as

$$C(t) = \frac{\nu(t) - \nu(\infty)}{\nu(0) - \nu(\infty)} \quad (5)$$

where $\nu(0)$, $\nu(t)$, and $\nu(\infty)$ are the energies of emission maxima in cm^{-1} at times 0, t, and ∞ after excitation. The time dependencies of the maxima of the fluorescence spectra were obtained by fitting a single Gaussian function at chosen delays of the streaks. The overall shape of the time-resolved fluorescence spectra remained the same at all times. The total spectral shift was about 8 nm toward the red from time zero to time infinity. For the reference compound, the shift was about 3 nm. The time evolution of the shift for the dansyl emission spectrum of the G1 dendrimer is shown in the inset of Figure 4.

Correlation functions for the dendrimers and the reference compound are shown in Figure 4, and the time constants and relative amplitudes of the exponential fits are collected in Table 1. $C(t)$ decay times for all dendrimer generations consisted of a faster component in the range of 15−30 ps and a longer component of 420−440 ps. For the reference compound, exponential decay components of 10 and 260 ps were obtained.

Time-dependent fluorescence anisotropies were calculated from fluorescence decays recorded in parallel and perpendicular directions with respect to the excitation polarization as follows

$$r(t) = \frac{I_{||}(t) - I_{\perp}(t)}{I_{||}(t) + 2I_{\perp}(t)} \quad (6)$$

Calculated anisotropy decay signals are presented in Figure 5 and the fitted time constants and the relative amplitudes in Table 2. In the fits given for pure G3 and G4 dendrimers, the longest anisotropy decay time was obtained from a separate time-correlated single-photon counting (TCSPC) measurement and was kept fixed during the fitting process. The reason for this was the short time window (1.6 ns) of the streak measurement to obtain reliable time constants for decay times longer than 1 ns. Two time domains could be resolved for the G1 and G2 dendrimers and the eosin G2 to G4 complexes. The fast components span the time window from 60 to 140 ps, and the slower components range from 300 to 1000 ps. For G3 and G4, third time constants of 1500 and 2600 ps, respectively, were taken from the TCSPC measurements. For the corresponding complexes, three exponential fits were also made by fixing the

TABLE 1: Time Constants and Relative Amplitudes of the Decay of Solvation Correlation Function for the Dansylated POPAM Dendrimers

sample	τ_1 (ps)	τ_2 (ps)
D[a]	10 (75%)	260 (25%)
G1	18 (61%)	420 (39%)
G2	26 (65%)	440 (35%)
G3	29 (57%)	430 (43%)
G4	16 (57%)	430 (43%)

[a] *N*-propyldansylamine.

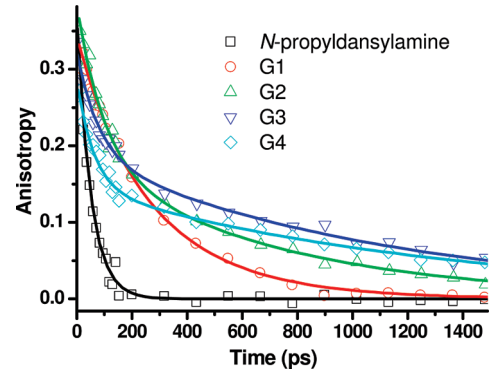

Figure 5. Fluorescence anisotropy decay traces of the dansylated POPAM dendrimers, G1 (red O), G2 (green Δ), G3 (blue ▽), and G4 (cyan ◇), and the reference compound (black □).

TABLE 2: Time Constants and Relative Amplitudes of the Dansyl Fluorescence Anisotropy Decays of Dansylated POPAM Dendrimers and the Corresponding Eosin Complexes

sample	τ_1 (ps)	τ_2 (ps)	τ_3 (ps)
D[a]	51 (100%)		
G1	140 (22%)	310 (78%)	
G2	100 (53%)	730 (47%)	(1100)[b]
G3	68 (36%)	500 (24%)	1500 (40%)[c]
G4	60 (46%)	1000 (41%)	2600 (13%)[c]
G2−eosin	54 (63%)	740 (37%)	
G3−eosin	93 (55%)	740 (45%)	
G3−eosin[d]	74 (50%)	530 (44%)	2250 (6%)
G4−eosin	110 (56%)	860 (44%)	
G4−eosin[d]	83 (43%)	460 (47%)	3900 (10%)

[a] *N*-propyldansylamine. [b] From TCSPC measurements. [c] From TCSPC measurements; this time constant was kept fixed when fitting the streak data. [d] Three component fit with a fixed τ_3 at 1.5 times that of the pure dendrimers.

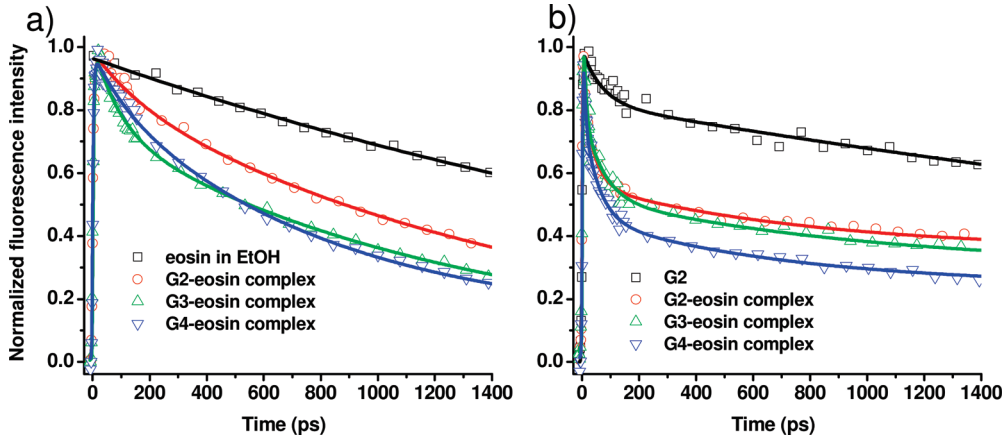

Figure 6. Magic angle fluorescence decay traces of the dendrimer−eosin complexes: G2−eosin (red O), G3−eosin (green Δ), and G4−eosin (blue ▽). (a) Eosin emission decays: eosin in solution (black □) and POPAM−eosin complexes at 554 nm. (b) Dansyl emission decays: dansylated G2 POPAM in solution (black □) and complexes at 499 nm.

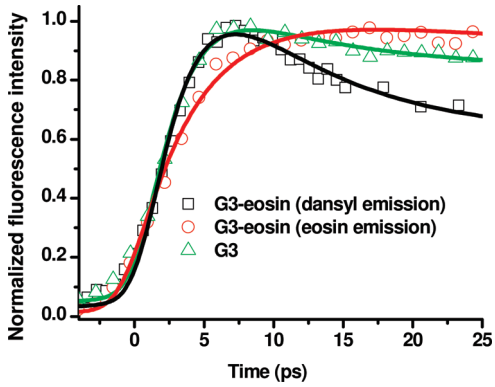

Figure 7. Early parts of the magic angle fluorescence rise and decay traces of the dansylated G3 POPAM dendrimer and its eosin complex: dansyl fluorescence decay of the pure dendrimer (green Δ), dansyl fluorescence decay of the dendrimer−eosin complex (black □), and eosin fluorescence decay of the dendrimer−eosin complex (red O). Kinetic traces were generated by integrating intensities over the emission bands of the streak camera images.

third time component to a value that was 1.5 times the value obtained experimentally for the pure dendrimers. This approach was supported by the results from MD simulations (Table 4).

B. POPAM−Eosin Complexes. For the POPAM−eosin complexes, time dependencies of the dansyl and eosin fluorescences were recorded simultaneously. Magic angle kinetics and anisotropy decay data were calculated for the dansyl and eosin emissions independently at selected wavelengths of the images. Eosin fluorescence decay curves for eosin−POPAM complexes and monomeric eosin in chloroform are shown in Figure 6a. The initial eosin fluorescence decay of the complexes is faster than that of eosin in solution. In Figure 6b are shown the dansyl fluorescence decay curves of the same complexes and the decay of G2 dendrimer as a reference. The initial fluorescence decay of the complexes goes much deeper than that of the G2 dendrimer, an indication of an additional relaxation channel being functional in the complexes. In Figure 7, the early parts of the kinetic traces of dansyl and eosin fluorescence signals of the G3−eosin complex are shown together with the signal from pure G3 POPAM. In the complexes, fluorescence from dansyls has an instant rise after excitation, whereas eosin fluorescence rises with the same rate as the dansyl fluorescence decays. We consider this as evidence of energy transfer from dansyls to eosin. Characteristic time constants of the studied complexes

TABLE 3: Time Constants of the Eosin and Dansyl Fluorescence Decays of the Dansylated POPAM−Eosin Complexes

sample	τ_1 (ps)	τ_2 (ps)	τ_3 (ps)
G2−eosin (dansyl)	5.6	67	4800
G2−eosin (eosin)	4.5 (rise)	170	1600
G3−eosin (dansyl)	7.7	76	4000
G3−eosin (eosin)	4.1 (rise)	90	1200
G4−eosin (dansyl)	8.0	72	3200
G4−eosin (eosin)	3.8 (rise)	120	800

are collected in Table 3. It is noted that time constants τ_3 have to be taken as tentative only because of the narrow streak time window.

Discussion

The magic angle fluorescence decays of the dendrimers studied consist of wavelength dependent picosecond components and wavelength-independent nanosecond components (Figures 2 and 3). For the reference compound *N*-propyldansylamine, the amplitude of the picosecond component is clearly much smaller than that for any of the dendrimers. These observations suggest that part of the dansyl excitation energy in the dendrimers is transferred into nonradiative channels. The change of the picosecond decay to a rise in the reference compound and the G1 and G2 dendrimers when going from the blue to the red end of the fluorescence spectrum was considered as evidence for an excited-state solvation process (Figure 3). The fast decay of the solvation correlation function $C(t)$ for the reference compound at about 10 ps was considered to give an upper limit of solvent relaxation around a single dansyl chromophore in the dendrimer. For the four dendrimers, almost identical biexponential $C(t)$ functions were obtained. The faster time constant, falling in the range of 15−30 ps, is assigned to the reorganization of the solvent around a single excited dansyl of the dendrimer. This interpretation relies on the similarity of the fast $C(t)$ components of the reference compound and the dendrimers. Just for comparison, the decay of the simulated autocorrelation function for the tumbling motion of chloroform has been reported to be in the range of 3−4 ps,[60] and experimental chloroform solvent reorganization is reported to be less than 3 ps.[61] It is noted that much slower internal motions of a dansyl of the dendrimer and the interaction between the excited dansyl and solvent molecules of the first solvation shell finally determine the solvent relaxation rate around an individual

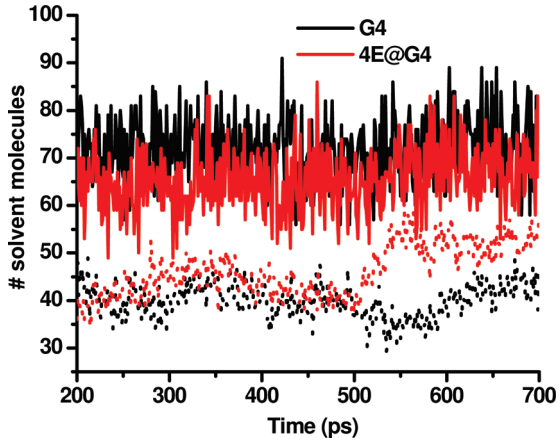

Figure 8. Instantaneous number of solvent molecules inside of dansylated G4 POPAM (black) and its eosin complex 4E@G4 (red) in $CHCl_3$ solution; the solid lines refer to the number of solvent molecules with at least one atom less than 2.8 Å away from an atom of the dendrimer, and the dotted lines refer to the number of solvent molecules inside of the dendrimer gyration radius, as displayed in Figure 11.

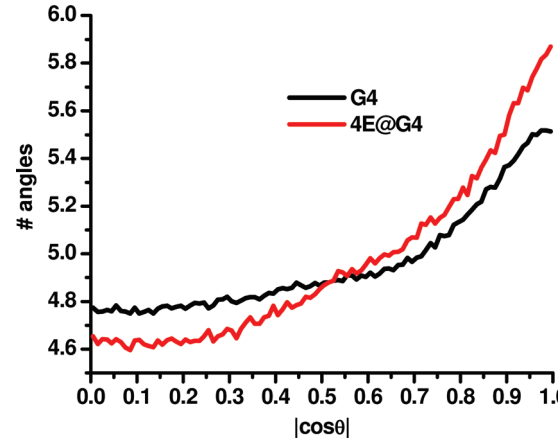

Figure 9. Averaged occurrence histogram of the modulus of the dansyl−dansyl orientation cosines as emerging from MD simulations for both dansylated G4 POPAM (black) and 4E@G4 (red). The orientation cosine between two dansyls is calculated on the basis of the angle between the two vectors perpendicular to the π-system of each dansyl. Within this convention, coplanarity entails a value of 1 for the modulus of the orientation cosine. Both distributions have been normalized to the total number of dansyl−dansyl orientation angles (496 for both G4 and 4E@G4).

dansyl.[62] The $C(t)$ components of 420−440 ps reflect relaxation on a much slower time scale. According to the present MD simulation, the dansyls of the G4 dendrimer experience both the bulk chloroform and the solvent that is trapped inside of the dendrimer. Several experimental results have suggested the existence of "freezing" of the solvent in a protein or in a micelle.[63,64] However, many other properties such as relative mass and size of the solute with respect to solvent, the shape and internal vibrational motions of the solute, and the interaction potential between the solute and the solvent have been found to contribute to slow solvation relaxation.[62−64] It is intriguing that for all of the dendrimers, independent of the generation, similar solvation correlation functions were obtained. The similarity may contrast with the notion that the density of dansyls, and thus the local microenvironment of an excited dansyl, is likely to differ in the G1 dendrimer (the dansyl chromophore is more like a monomeric dansyl in solution) and in the G4 dendrimer (the excited dansyl experiences interaction with its neighbor dansyls as well as the solvent shell). One would therefore have expected a slightly different solvation dynamics for each generation, at least for the long time component. An explanation may be the large solvent density and high mobility inside of the dendrimer. As shown in Figure 8, MD simulations suggest that up to 70 solvent molecules ($CHCl_3$) penetrate the inside of the G4 POPAM dendrimer. Solvent molecules then efficiently surround the dansyls whether inside or in the periphery of the dendritic structure, preventing dansyls from interacting with each other and making the solvation relaxation independent of the dansyl density or the dendrimer generation. If we are to rely on the MD results that indicate high mobility of the solvent molecules also inside of the dendrimer, we are obliged to conclude that the slow component is not due to "freezing" of the solvent inside of the dendrimer but to the other effects mentioned above that possibly contribute to the slow component. With the present results in hand, we are not able to discuss these effects in any further detail.

Two characteristic time constants of fluorescence anisotropy decays of G1 and G2 were resolved. Three time constants were resolved for G3 and G4, respectively, using the fitting procedure described above. It is noted that the evaluated time constants depend on initial fitting parameters, and a 20% error margin is estimated. However, the results clearly allow identification of three time domains at 60−140, 300−1000, and 1500−2600 ps.

The anisotropy decay of the reference compound was monoexponential and faster than the fastest decay of any of the dendrimers. This decay is assigned to rotational diffusion of *N*-propyldansylamine in chloroform and gives the time frame for the rotating dansyls in the dendrimers. The observed rotational time constant of 51 ps is consistent with the value of 50 ps measured by Zhong et al.[65] for dansyl chloride in methanol. Comparison of the overall rotation time of the reference compound and the fastest resolved anisotropy time constants of the dendrimers suggests that the latter are due to "freely" moving dansyl reorientations experiencing friction mainly from the bulk solvent. The fast anisotropy time constants, assigned to terminal group motions in the dendrimers, are slightly longer than the rotational diffusion time of the reference compound, which one would expect since dansyls are not totally free to rotate in the dendrimers. The observed trend for the short anisotropy component from G1 to G4 dendrimers (Table 2), increased rate of orientation motion of the terminal groups toward larger dendrimers, is at least qualitatively in line with the results of the MD simulation by Karatasos et al.,[45] which indicate that the reorientational time τ_{av} for the G3, G4, and G5 dendrimers seems to shorten slightly for the shell most distant from the center (see Figure 12, ref 45). Another explanation could be higher "solvent inertia" around the terminal groups in the smaller dendrimers than that in the larger dendrimers, slowing down the motion in small dendrimers.

Dansyl−dansyl relative orientations from MD simulation also suggest almost free rotational motion for the dansyl fragments. In fact, as is evident from analysis of the relative orientations among the dansyl units (see Figure 9), the distribution of the dansyl−dansyl orientations seems to be rather homogeneous, and the MD trajectories do not suggest any preferential orientation. When considering that the total number of dansyl−dansyl relative orientations is 496 for G4, the deviations displayed in Figure 9 are objectively negligible, in full agreement with the almost free nature of the dansyl rotational motion. (See the movie of internal motions of the G4 dansylated POPAM dendrimer in chloroform in Supporting Information, G4_POPAM_movie).

According to theoretical simulations, the orientational relaxation of the dendrimers originates from three different processes,

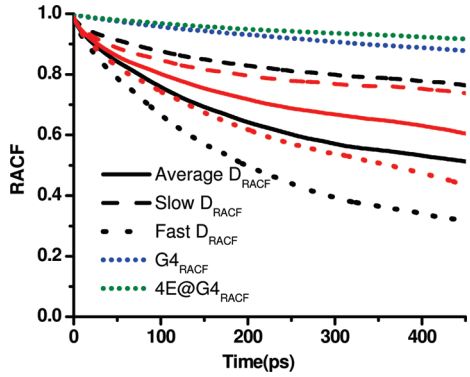

Figure 10. Calculated dansyl rotational autocorrelation function (D_{RACF}) for G4 POPAM (black) and its eosin complex 4E@G4 (red). Fast and slow components are averaged from dansyls, which have D_{RACF} lower or higher than the average of all dansyls. Global dendrimer rotations ($G4_{RACF}$) and ($4E@G4_{RACF}$) are shown for comparison.

(i) the rotation of the whole dendrimer, (ii) the motions of the internal shells, and (iii) motions of the terminal chromophores.[43,45] Karatasos et al.[45] and Markelov et al.[43] predicted that the relaxation of the outermost shell is dominated by the local motions of the end groups and has only minor dependence on the dendrimer generation. However, our experimental fluorescence anisotropy decay showed a clear dependence on the size of the dendrimer and triggered the need for longer simulation of the MD trajectories, which was then extended to >2 ns for G4 and its complex with four eosins (4E@G4). A summary of the analysis of the dansyl motions and overall rotation of G4 and 4E@G4 are shown in Figure 10 (for further details of the analysis, see the Supporting Information). Analysis of single dansyl trajectories reveals that the distribution of the orientation decay times of the 32 dansyls is rather inhomogeneous, which suggests that each dansyl experiences strong dependence on the given hosting environment in both G4 and 4E@G4. To qualitatively separate the dansyl motions, individual dansyl D_{RACF}'s were divided into two groups according to their D_{RACF} behavior. Dansyls moving faster than the average of all 32 dansyls were averaged to fast dansyls. Dansyls moving slower than the average of all 32 dansyls were averaged to slow dansyls. The D_{RACF} averages of fast and slow dansyls are depicted in Figure 10. It is evident that dansyl motions with the division adopted may be intuitively assigned to "fast" dansyl motions and to "slow", more hindered motions of back-folded dansyls. Notably, the correlation time of the slower dansyl groups is rather close to the global dendrimer rotation time scale, suggesting that back-folding may effectively embed dansyls in the dendrimer.

Despite the limitation of the data set building on the semiquantitative convergence of D_{RACF} and D_{G4} (see Supporting Information), it is possible to estimate the orientation relaxation time by extrapolation of the calculated D_{RACF} and D_{G4}. While the decay of D_{G4} can be rather accurately fitted by a single exponential, the calculated D_{RACF}'s show a biexponential decay, with a faster (τ_1) component contributing less than 20% ($c_1 < 0.2$) to the total D_{RACF} decay. This originates from contamination of the dansyl torsional angle by (faster) torsion movement of the aliphatic dendrimer dendrons. Due to the limitation of the MD data set, and the ensuing impossibility to substantially extend D_{RACF}, it is not straightforward to eliminate the τ_1 contamination by Fourier transform analysis. On this basis, effective relaxation times (τ^*) were estimated by setting the extrapolated $D_{RACF}(\tau^*) = e^{-1}$. The results are given in Table 4.

The time constants of Table 4 are roughly two times longer than the corresponding experimentally determined constants of Table 2. The adopted MM3 force field overestimates the density of $CHCl_3$ by 15%, and this is likely to play a role in the overestimated relaxation rates of the dendrimer rotation. Thus, despite overestimation of the experimental time constants, the data in Table 4 nevertheless recover the measured trends (τ_1(G4) < τ_1(4E-G4); τ_2(G4) > τ_2(4E@G4)). Additionally, the ratios between τ_1/τ_2 for G4 and 4E@G4 from the simulation of 2.11 and that from the experiments of 3.00 are in acceptable agreement, thus backing up the adopted procedure.

TABLE 4: Extrapolated Decay Time (ps) for Global Dendrimer Rotation (τ_R) and Fast (τ_1) and Slow (τ_2) Dansyl Motion

	τ_1	τ_2	τ_R
G4	332	2650	4434
4E@G4	566	2141	7520

Measured anisotropy decays represent averages of the motions of a large number of dansyls in the excitation volume. The time-resolved anisotropy results of Table 2 indicate division of dansyl orientations in fast and slow motions as predicted by the MD simulations. The fast dansyl motions fall in the time domain from 60 to 140 ps, and the slow dansyl motions fall in from the 300 to 1000 ps time domain. The longest anisotropy decay component of the pure dendrimers is clearly correlated to the size of the molecule and is hence assigned rotational diffusion of the dendrimer in solution. For G1 and G2, variations in dansyl motions are likely to be smaller than that in G3 or G4, where back-folding may take place. Hence, the fast anisotropy components of G1 and G2 are assigned to "free" dansyl motion and the long components to overall rotation. For G2, two overall time constants are given in Table 2, one from streak camera measurements and one from the TCSPC measurements. The latter value is to be trusted more as the time window of the streak camera measurement was limited. For this same reason, the longest time constants for G3 and G4 were taken from TCSPC measurements and kept fixed when fitting the streak camera data. After this procedure, the slow dansyl motion time constants discussed above could be resolved.

With the assignment that the longest anisotropy decay times reflect overall rotational motion of the dendrimer, we can estimate the dendrimer volume by using the hydrodynamic Stokes−Einstein−Debye model[66]

$$\tau_{rot} = \frac{\eta V}{kT} \tag{7}$$

In eq 7, τ_{rot} is the rotation correlation time of the molecule, η is the viscosity of the solvent, V is the hydrodynamic volume of the molecule, and k is the Boltzmann constant. Equation 7 is valid for the spherical molecules with the "stick" boundary condition. Stick models, where the first solvent layer moves with the molecule, can be assumed to be valid for large molecules such as dendrimers, whereas the slip boundary condition is more appropriate for description of rotational motion of small molecules in nonpolar solvents.[66] The assumption of a spherical shape for soft dendrimers is founded because of their flexible nature and fuzzy molecular structure. The fast internal motions of the terminal groups mean that on time scales longer than these motions, the distribution of nonspherical configurations averages out into a spherical shape. It has been shown that the moment of inertia aspect ratio approaches that of a sphere as the dendrimer size increases.[45,67,68] By using eq 7 and the resolved long anisotropy decay times, hydrodynamic volumes of 2.3, 7.9, 10.5, and 18.6 nm^3 and hydrodynamic radii of 0.81, 1.24, 1.36, and 1.64 nm from G1 to G4 are obtained.

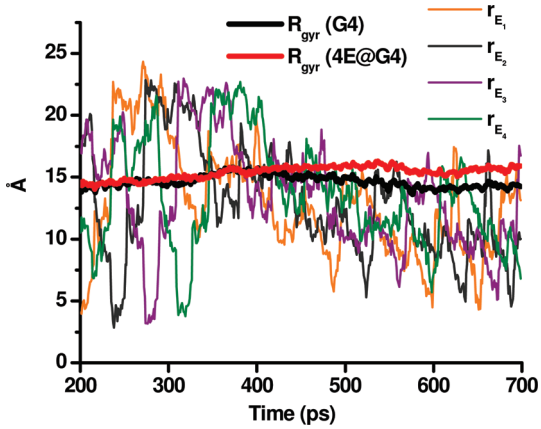

Figure 11. Gyration radius of dansylated G4 POPAM and its eosin complex 4E@G4 in $CHCl_3$ and the distances of mass centers of each eosin from the mass center of G4 obtained from MD simulations.

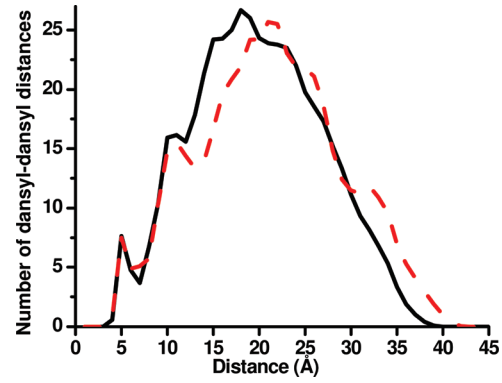

Figure 12. Averaged dansyl−dansyl distance occurrence histograms for G4 (black, solid) and the G4−eosin complex (red, dash) from MD simulations. Both distributions have been generated on the basis of 1 Å sampling grids and eventually normalized to the total number of dansyl−dansyl distances (496 for both G4 and 4E@G4).

The increase in volume is certainly much smaller than one would have expected from symmetric 2D rigid structures, and the results may be considered as experimental evidence of substantial back-folding of the terminal groups of the dendrimers, in particular, in the higher-generation dendrimers. The hydrodynamic radius of 1.6 nm obtained for G4 compares nicely to the radius of gyration of 1.5 nm obtained from the simulation (Figure 11). Our results are in accord with previous theoretical and experimental studies[11,12,37] for POPAM dendrimers, and the hydrodynamic volumes are comparable to the volumes of 5.8, 12.6, and 17.4 nm^3 for G2, G3, and G4, respectively, in dichloromethane determined by Vicinelli et al.[69]

Besides vanishing by overall rotation, fluorescence anisotropy may disappear due to motions of individual dansyls as well as due to excitation energy transfer (EET) between dansyls. In the higher-generation dendrimers, EET is more likely to become an important dansyl−dansyl relaxation channel than in the smaller ones. In order to obtain an estimate of EET rates in the four POPAM generations, the Förster rate equation[66] was used

$$k_{ET}(r) = \frac{8.8 \times 10^{-5} \kappa^2 \Phi_D J}{\tau_D n^4 r^6} \qquad (8)$$

In eq 8, κ is the orientation factor (assumed to have a value of $\kappa^2 = 2/3$), Φ_D and τ_D are the quantum yield and the lifetime of the donor fluorescence in the absence of the acceptor (0.4 and 10 ns, respectively, were used), n is the refractive index of the solvent (1.446), J is the overlap integral of the donor emission spectrum and the acceptor absorption spectrum, and r is the distance between the acceptor and donor in Ångströms. Values of Φ_D and τ_D for dansyl fluorescence could not be found for chloroform solutions, but the parameters do not vary much from solvent to solvent.[9] From eq 8, dansyl−dansyl distances of 4.5−3.9 Å were estimated by assuming that the 140−62 ps anisotropy decays in G1 to G4 dendrimers describe dansyl−dansyl EET with $k_{ET} = \tau_{aniso}^{-1}$. These values should be understood as rough estimates of dansyl−dansyl average distances, with the assumption that anisotropy decays are due to Förster energy transfer. However, the dansyl−dansyl distance histogram obtained from MD simulations for G4 POPAM gives only a very small fraction of dansyl−dansyl distances of 5 Å, and most of the dansyls have their closest neighbor much further away, the mean distance being about 20 Å (Figure 12). In the eosin−POPAM G4 complex, the average of the dansyl−dansyl distances is even larger at about 21 Å, which, according to simulation, also means that the number of solvent molecules inside of the complex increases as compared to pure dendrimers (Figures 8 and 12). According to the Förster model, a 5 Å interdansyl distance leads to a 270 ps EET time constant, and a 6 Å distance leads to a 800 ps rate. Therefore, the fast anisotropy decay observed for the dendrimers must describe internal motion of the dansyls and not EET between the dansyls. There is a possibility that EET between dansyls may occasionally take place if dansyl motions provide favorable orientations for EET, but the probability of such occasions according to MD simulations is practically zero.

Dansyl to eosin excitation energy-transfer rates were determined from dansyl fluorescence decay and eosin fluorescence rise signals of the POPAM−eosin complexes. Figure 7 shows early parts of fluorescence kinetics for pure G3 POPAM (dansyl emission) and the G3 POPAM−eosin complex after exciting dansyls selectively with 400 nm femtosecond pulses. The rise times of dansyl emissions (pure dendrimer and the complex) are instrument-limited. Dansyl fluorescence decay of the complex is clearly faster than that of the pure dendrimer, an indication of excitation energy leakage due to a mechanism other than dansyl−dansyl EET. As the rise time of the eosin fluorescence nearly perfectly matches the dansyl decay time, we conclude that EET takes place directly from an excited dansyl to eosin. Similar responses were observed also for the other POPAM−eosin complexes; the characteristic time constants ranged from 4 to 8 ps. These results are in agreement with our previous transient absorption spectroscopy studies carried out at about 80 fs time resolution, where, besides a very fast 100 fs EET time component, 1 and 6 ps EET rates were resolved.[54] Since the time resolution of the present study was only about 3 ps, it is most likely that the 1 and 6 ps components recorded previously at much better time resolution will be averaged into single time constants ranging from 4 to 8 ps obtained with lower time resolution.

In dansylated POPAM−eosin complexes, EET from dansyls to eosin is the rate-determining factor of dansyl fluorescence decay since the overlap integral of dansyl fluorescence and eosin absorption is 4 orders of magnitude larger than that for dansyl absorption and dansyl fluorescence. For 50% energy-transfer efficiency, the Förster radius for dansyl−eosin EET was estimated to be 44 Å as compared to 9.1 Å for dansyl-to-dansyl EET. The fact that the distances of eosins from the center of mass of the largest dendrimer according to the MD simulations (Figure 11) are fluctuating at around 15 Å and that most dansyls are much closer to eosins than this distance means that energy is transferred efficiently from excited dansyls to eosins. We can

estimate that the optical excitation from the most distant dansyl will reach the eosin without involvement of much slower dansyl-to-dansyl EET. (See the movie of internal motions of the eosin-dansylated G4 POPAM dendrimer complex with four eosins in chloroform in the Supporting Information, E4@G4POPAM_movie).

In solution, equilibrium prevails between free dendrimers, free guests, and the complex. The number of eosins in the complex varies from zero to one for G2, from zero to three for G3, and from zero to six for G4.[48] Figure 6b shows that after about 500 ps, the dansyl fluorescence decay curves of the complexes and the free G2 dendrimer become nearly parallel. The nanosecond decays most likely arise from dansyl emission of the free POPAMs in solution.

Fits of dansyl fluorescence anisotropy decays of the complexes with two exponentials gave nearly constant long time component for generations G2−G4 (Table 2). Experimental long anisotropy time constants τ_3 could not be resolved from the streak data as this time domain falls far away from the predicted overall rotation times. Since the single-photon counting data were not available for the complexes, τ_3 was fixed to value 1.5 times that of the pure dendrimers based on an approximate ratio of the overall rotation times from MD simulations. The value of the longest component had only a minor effect on the shorter time constants of the complexes, justifying the more or less arbitrary choice of the τ_3. In the complexes, the short dansyl anisotropy relaxation time seems to increase slightly when moving from G2 to G4 complexes (Table 2); opposite behavior was observed for pure dendrimers. In qualitative accordance with the simulations, anisotropy results indicate that the fast dansyl motions of G4 are actually faster than those in 4E@G4. It thus emerges that eosins hinder fast rotation of the dansyl fragments. Interestingly, and in accordance with the measured τ_2 values given in Table 2, slow dansyl motions are modeled to be slower in G4 than those in 4E@G4. This is due to the more compact structure of G4, which increases the steric hindrance to back-folded dansyls motion with respect to 4E@G4. In the presence of the eosins, the dendrimer structure is left more open, which accordingly reduces restriction to back-folded dansyl motion, hence the shorter τ_2 for 4E@G4. The open structure of the complex also slows down the overall rotation of the complex compared to that of the pure dendrimer (see Table 4). It remains an open question why the short anisotropy component in pure G2 dendrimer should be two times slower than that in the G2−eosin complex (Table 2). We note that the results from anisotropy decays of the complexes should be treated with caution because of the fast EET to eosin. There may always be also free dendrimers present in solution, and their fluorescence in the dansyl region is more intense than dansyl fluorescence in complexes where excitation is transferred effectively to eosin.

Fluorescence anisotropy decays of dendrimer-bound eosin(s) were much faster than the dansyl anisotropy decays, reaching a level below 0.1 in about 5 ps, the time scale of energy transfer from dansyls to eosin. Due to large overlap of eosin absorption and eosin fluorescence, EET between eosins is also likely to take place in the complexes containing more than one eosin. Besides the fast rise times of 4−8 ps for eosin fluorescence, the decay components from 90 to 170 ps and 800 to 1600 ps were resolved for G2 to G4 complexes, respectively (Table 3). As compared to a single exponential eosin fluorescence lifetime of 3.6 ns in solution,[70,71] the faster eosin decays observed in POPAM complexes must be due to quenching induced by interactions with dendrimer.

Conclusions

Time-resolved fluorescence spectra of four dansylated POPAM G1−G4 dendrimers and their eosin complexes in solution were studied. Time-dependent shifts of the fluorescence spectra of the dansylated POPAMs were interpreted in terms of excited-state solvation relaxation. Solvation correlation functions of the dendrimers were characterized by fast, 10−30 ps, and slow, ∼420−440 ps, exponential components, a behavior commonly met in micelle and protein solvation. The results suggest that solvent molecules efficiently surround the dansyls whether inside of or in the periphery of the dendritic structure, preventing dansyls from interacting with each other and making the solvation relaxation almost independent of the dendrimer generation.

Dansyl fluorescence anisotropy decays of the dendrimers in general showed biexponential behavior. The fast decay component in the time domain from 60 to 140 ps is related to relatively "free" dansyl orientational motion of the dendrimers. Monoexponential anisotropy decay of 51 ps of the reference compound, *N*-propyldansylamine, was considered as an upper rate limit for nearly freely moving dansyls of the dendrimers. It was shown that dansyl−dansyl EET could not give rise to fast anisotropy components. The slower anisotropy component falls in the time domain from 300 to 1000 ps. For G1 and G2, where back-folding does not play an important role, these were assigned to overall rotation of the dendrimer. The reorientational motions falling in the slow time window of 510 and 1000 ps for the G3 and G4 dendrimers, respectively, are related to reorientational motion of the back-folded dansyls. A third anisotropy component was identified for the G3 and G4 POPAMs from TCSPC experiments, suggesting overall rotational lifetimes of the G3 and G4 dendrimers of 1500 and 2600 ps, respectively. This assignment was supported by the results of the extended MD simulations. The hydrodynamic radii of the dendrimers were evaluated by using the Stokes−Einstein hydrodynamic model with the stick boundary condition implying a much slower increase of the dendrimer volume when moving from G2 to G4 generation than would be expected from rigid two-dimensional structures.

Time-resolved fluorescence measurements of POPAM−eosin complexes suggest energy transfer from dansyl to eosin(s) to occur in 4−8 ps picoseconds, in accord with our previous transient absorption measurements. EET from excited dansyls to eosin(s) could be explained within the Förster picture without considering dansyl-to-dansyl EET. The fast dansyl motions were observed to be slower in the eosin−POPAM complexes than those in pure dendrimers due to hindrance of the dansyl motion by eosin. On the other hand, the slower dansyl motions were found to be faster in the more open structure of the G3 and G4 complexes than those in the more compact structure of the pure dendrimers. The overall rotational lifetimes of the POPAM−eosin complexes could not be extracted from the experimental streak data as the time window of the measurement was limited. The simulations, however, clearly suggest that the overall rotational lifetimes of the complexes are substantially longer than the corresponding lifetimes for the pure POPAMs.

Acknowledgment. J.A. acknowledges the scholarship from LASKEMO graduate school funded by the ministry of education of Finland. Ngong Beyeh Kodiah is acknowledged for the synthesis of *N*-propyldansylamine reference compound. Pasi Myllyperkiö is acknowledged for helping in global fitting of the kinetic data. Financial support from Academy of Finland under the TULE and the FinNano programs (Contracts 205475 and 118040) is acknowledged.

Supporting Information Available: MD simulation movies of internal motions of dansylated G4 POPAM and the G4 POPAM−eosin complex in chloroform. This material is available free of charge via the Internet at http://pubs.acs.org.

References and Notes

(1) Bosman, A. W.; Janssen, H. M.; Meijer, E. W. *Chem. Rev.* **1999**, *99*, 1665–1688.

(2) Zeng, F.; Zimmerman, S. C. *Chem. Rev.* **1997**, *97*, 1681–1712.

(3) Grayson, S. M.; Fréchet, J. M. J. *Chem. Rev.* **2001**, *101*, 3819–3868.

(4) Crampton, H. L.; Simanek, E. E. *Polym. Int.* **2007**, *56*, 489–496.

(5) Gupta, U.; Pharm, B.; Agashe, H. B.; Pharm, M.; Asthana, A.; Jain, N. K. *Nanomedicine* **2006**, *2*, 66–73.

(6) Myc, A.; Majoros, I. J.; Thomas, T. P.; Baker, J. R., Jr. *Biomacromolecules* **2007**, *8*, 13–18.

(7) Dhanikula, R. S.; Hildgen, P. *Bioconjugate Chem.* **2006**, *17*, 29–41.

(8) Vögtle, F.; Gestermann, S.; Kauffmann, C.; Ceroni, P.; Vicinelli, V.; De Cola, L.; Balzani, V. *J. Am. Chem. Soc.* **1999**, *121*, 12161–12166.

(9) Li, Y.; Chan, L.; Tyer, L.; Moody, R. T.; Himel, C. M.; Hercules, D. M. *J. Am. Chem. Soc.* **1975**, *97*, 3118–3126.

(10) Ren, B.; Gao, F.; Tong, Z.; Yan, Y. *Chem. Phys. Lett.* **1999**, *307*, 55–61.

(11) Ballauff, M. In *Dendrimers III — Design, Dimension, Function*; Springer-Verlag: Berlin, Germany, 2001; Vol. 212, pp 177−194.

(12) Rosenfeldt, S.; Dingenouts, N.; Ballauff, M.; Werner, N.; Vögtle, F.; Lindner, P. *Macromolecules* **2002**, *35*, 8098–8105.

(13) Rosenfeldt, S.; Dingenouts, N.; Potschke, D.; Ballauff, M.; Berresheim, A. J.; Mullen, K.; Lindner, P.; Saalwachter, K. *J. Lumin.* **2005**, *111*, 225–238.

(14) Likos, C. N.; Rosenfeldt, S.; Dingenouts, N.; Ballauff, M.; Lindner, P.; Werner, N.; Vögtle, F. *J. Chem. Phys.* **2002**, *117*, 1869–1877.

(15) Balzani, V.; Ceroni, P.; Maestri, M.; Saudan, C.; Vicinelli, V. In *Dendrimers V*; Springer-Verlag: Berlin, Germany, 2003; Vol *228*, pp 159−191.

(16) Balzani, V.; Ceroni, P.; Gestermann, S.; Kauffmann, C.; Gorka, M.; Vögtle, F. *Chem. Commun.* **2000**, 853–854.

(17) Furuta, P.; Brooks, J.; Thompson, M. E.; Fréchet, J. M. J. *J. Am. Chem. Soc.* **2003**, *125*, 13165–13172.

(18) Saudan, C.; Balzani, V.; Gorka, M.; Lee, S.; Maestri, M.; Vicinelli, V.; Vögtle, F. *J. Am. Chem. Soc.* **2003**, *125*, 4424–4425.

(19) Serin, J. M.; Brousmiche, D. W.; Fréchet, J. M. J. *J. Am. Chem. Soc.* **2002**, *124*, 11848–11849.

(20) Wang, B.; Zhang, X.; Jia, X.; Li, Z.; Ji, Y.; Yang, L.; Wei, Y. *J. Am. Chem. Soc.* **2004**, *126*, 15180–15194.

(21) Precup-Blaga, F. S.; Garcia-Martinez, J. C.; Schenning, A. P. H. J.; Meijer, E. W. *J. Am. Chem. Soc.* **2003**, *125*, 12953–12960.

(22) Saudan, C.; Ceroni, P.; Vicinelli, V.; Maestri, M.; Balzani, V.; Gorka, M.; Lee, S.; van Heyst, J.; Vögtle, F. *Dalton Trans.* **2004**, 1597–1600.

(23) Atas, E.; Peng, Z.; Kleiman, V. D. *J. Phys. Chem. B* **2005**, *109*, 13553–13560.

(24) Kleiman, V. D.; Melinger, J. S.; McMorrow, D. *J. Phys. Chem. B* **2001**, *105*, 5595–5598.

(25) Wang, Y.; He, G. S.; Prasad, P. N.; Goodson, T., III. *J. Am. Chem. Soc.* **2005**, *127*, 10128–10129.

(26) Ranasinghe, M. I.; Hager, M. W.; Gorman, C. B.; Goodson, T., III. *J. Phys. Chem. B* **2004**, *108*, 8543–8549.

(27) Ahn, T. S.; Thompson, A. L.; Bharathi, P.; Mueller, A.; Bardeen, C. J. *J. Phys. Chem. B* **2006**, *110*, 19810–19819.

(28) Melnikov, S. M.; Yeow, E. K. L.; Uji-i, H.; Cotlet, M.; Mullen, K.; DeSchryver, F. C.; Enderlein, J.; Hofkens, J. *J. Phys. Chem. B* **2007**, *111*, 708–719.

(29) Lor, M.; Viaene, L.; Pilot, R.; Fron, E.; Jordens, S.; Schweitzer, G.; Weil, T.; Müllen, K.; Verhoeven, J. W.; Van der Auweraer, M. V.; De Schryver, F. C. *J. Phys. Chem. B* **2004**, *108*, 10721–10731.

(30) Hania, P. R.; Heijs, D. J.; Bowden, T.; Pugzlys, A.; Van Esch, J.; Knoester, J.; Duppen, K. *J. Phys. Chem. B* **2004**, *108*, 71–81.

(31) Hofkens, J.; Latterini, L.; De Belder, G.; Gensch, T.; Maus, M.; Vosch, T.; Karni, Y.; Schweitzer, G.; De Schryver, F. C.; Hermann, A.; Müllen, K. *Chem. Phys. Lett.* **1999**, *304*, 1–9.

(32) Yeow, E. K. L.; Ghiggino, K. P.; Reek, J. N. H.; Crossley, M. J.; Bosman, A. W.; Schenning, A. P. H. J.; Meijer, E. W. *J. Phys. Chem. B* **2000**, *104*, 2596–2606.

(33) Larsen, J.; Andersson, J.; Polívka, T.; Sly, J.; Crossley, M. J.; Sundström, V.; Åkesson, E. *Chem. Phys. Lett.* **2005**, *403*, 205–210.

(34) Wang, B.; Zhang, X.; Jia, X.; Li, Z.; Ji, Y.; Wei, Y. *J. Polym. Sci., Part A: Polym. Chem.* **2005**, *43*, 5512–5519.

(35) Adronov, A.; Fréchet, J. M. J. *Chem. Commun.* **2000**, 1701–1710.

(36) Brousmiche, D. W.; Serin, J. M.; Fréchet, J. M. J.; He, G. S.; Lin, T.; Chung, S.; Prasad, P. N.; Kannan, R.; Tan, L. *J. Phys. Chem. B* **2004**, *108*, 8592–8600.

(37) Ballauff, M.; Likos, C. N. *Angew. Chem., Int. Ed.* **2004**, *43*, 2998–3020.

(38) Cavallo, L.; Fraternali, F. *Chem.—Eur. J.* **1998**, *4*, 927–934.

(39) Welch, P.; Muthukumar, M. *Macromolecules* **1998**, *31*, 5892–5897.

(40) Lee, I.; Athey, B. D.; Wetzel, A. W.; Meixner, W.; Baker, J. R., Jr. *Macromolecules* **2002**, *35*, 4510–4520.

(41) Topp, A.; Bauer, B. J.; Klimash, J. W.; Spindler, R.; Tomalia, D. A.; Amis, E. J. *Macromolecules* **1999**, *32*, 7226–7231.

(42) Lyulin, A. V.; Davies, G. R.; Adolf, D. B. *Macromolecules* **2000**, *33*, 6899–6900.

(43) Markelov, D. A.; Lyulin, S. V.; Gotlib, Yu. Ya.; Lyulin, A. V.; Matveev, V. V.; Lähderanta, E.; Darinskii, A. A. *J. Chem. Phys.* **2009**, *130*, 044907.

(44) Lyulin, S. V.; Darinskii, A. A.; Lyulin, A. V.; Michels, M. E. J. *Macromolecules* **2004**, *37*, 4676–4685.

(45) Karatasos, K.; Adolf, D.; Davies, G. R. *J. Chem. Phys.* **2001**, *115*, 5310–5318.

(46) Meltzer, A. D.; Tirrel, D. A.; Jones, A. A.; Inglefield, P. T.; Hedstrand, D. M.; Tomalia, D. A. *Macromolecules* **1992**, *25*, 4541–4548.

(47) Starck, B.; Stuehn, B.; Frey, H.; Lach, C.; Lorenz, K.; Frick, B. *Macromolecules* **1998**, *31*, 5415–5423.

(48) Balzani, V.; Ceroni, P.; Gestermann, S.; Gorka, M.; Kauffmann, C.; Vögtle, F. *Tetrahedron* **2002**, *58*, 629–637.

(49) Larsen, J.; Brüggemann, B.; Sly, J.; Crossley, M. J.; Sundström, V.; Åkesson, E. *Chem. Phys. Lett.* **2006**, *433*, 159–164.

(50) Larsen, J.; Brüggemann, B.; Khoury, T.; Sly, J.; Crossley, M. J.; Sundström, V.; Åkesson, E. *J. Phys. Chem. A* **2007**, *111*, 10589–10597.

(51) Neuwahl, F. V. R.; Righini, R.; Adronov, A.; Malenfant, P. R. L.; Fréchet, J. M. J. *J. Phys. Chem. B* **2001**, *105*, 1307–1312.

(52) Balzani, V.; Vögtle, F. *C. R. Chim.* **2003**, *6*, 867–872.

(53) Schenning, A. P. H. J.; Peeters, E.; Meijer, E. W. *J. Am. Chem. Soc.* **2000**, *122*, 4489–4495.

(54) Aumanen, J.; Lehtovuori, V.; Werner, N.; Richardt, G.; van Heyst, J.; Vögtle, F.; Korppi-Tommola, J. *Chem. Phys. Lett.* **2006**, *433*, 75–79.

(55) Archut, A.; Gestermann, S.; Hesse, R.; Kauffmann, C.; Vögtle, F. *Synlett* **1998**, 546–548.

(56) Ceroni, P.; Laghi, I.; Maestri, M.; Balzani, V.; Gestermann, S.; Gorka, M.; Vögtle, F. *New J. Chem.* **2002**, *26*, 66–75.

(57) Teobaldi, G.; Zerbetto, F. *J. Am. Chem. Soc.* **2003**, *125*, 7388–7393.

(58) Vögtle, F.; Gestermann, S.; Kauffmann, C.; Ceroni, P.; Vicinelli, V.; Balzani, V. *J. Am. Chem. Soc.* **2000**, *122*, 10398–10404.

(59) Maroncelli, M.; Fleming, G. R. *J. Chem. Phys.* **1987**, *86*, 6221–6239.

(60) Rothschild, W. G. *Mol. Phys.* **2006**, *104*, 1421–1427.

(61) Nibbering, E. T. J.; Elsaesser, T. *Appl. Phys. B* **2000**, *71*, 439–441.

(62) Egorov, S. A.; Denny, R. A.; Reichman, D. R. *J. Chem. Phys.* **2002**, *116*, 5080–5089.

(63) Peon, J.; Pal, S. K.; Zewail, A. H. *Proc. Natl. Acad. Sci. U.S.A.* **2002**, *99*, 10964–10969.

(64) Banerjee, D.; Pal, S. K. *Chem. Phys. Lett.* **2008**, *451*, 237–242.

(65) Zhong, D. P.; Pal, S. K.; Zewail, A. H. *ChemPhysChem* **2001**, *2*, 219–227.

(66) Lakowicz, J. R. *Principles of Fluorescence Spectroscopy*; Kluwer Academic/Plenum Publishers: New York, 1999.

(67) Maiti, P. K.; Cagin, T.; Wang, G.; Goddard, W. A. *Macromolecules* **2004**, *37*, 6236–6254.

(68) Paulo, P. M. R.; Lopes, J. N. C.; Costa, S. M. B. *J. Phys. Chem. B* **2007**, *111*, 10651–10664.

(69) Vicinelli, V.; Bergamini, G.; Ceroni, P.; Balzani, V.; Vögtle, F.; Lukin, O. *J. Phys. Chem. B* **2007**, *111*, 6620–6627.

(70) Fleming, G. R.; Knight, A. W. E.; Morris, J. M.; Morrison, R. J. S.; Robinson, G. W. *J. Am. Chem. Soc.* **1977**, *99*, 4306–4311.

(71) Jena, K. C.; Bisht, P. B. *Chem. Phys.* **2005**, *314*, 179–188.

JP902906Q